Ocean Engineering 268 (2023) 113425

Contents lists available at ScienceDirect

Ocean Engineering

journal homepage: www.elsevier.com/locate/oceaneng

# Automatic dock-to-dock control system for surface vessels using bumpless transfer

Jens Emil Walmsness [a,b,*], Håkon Hagen Helgesen [a], Stefan Larsen [a,b], Giorgio Kwame Minde Kufoalor [b], Tor Arne Johansen [a]

[a] NTNU Centre for Autonomous Marine Operations and Systems, Department of Engineering Cybernetics, Norwegian University of Science and Technology, O. S. Bragstads plass 2D, 7491 Trondheim, Norway

[b] Maritime Robotics AS, Brattørkaia 11, 7010 Trondheim, Norway

ARTICLE INFO

*Keywords:*
Automatic control
Bumpless transfer
Guidance
Unmanned surface vessels

ABSTRACT

This paper proposes and demonstrates an automatic steering system designed for passenger ferries with dock-to-dock capabilities. The method consists of a modular control architecture and bumpless transfer transition strategies that enable the implementation of different independent controllers for different vessel operational phases. The method is expressed as a state machine and divides the ferry operations into three different phases, UNDOCKING, TRANSIT, and DOCKING. The proposed modular architecture allows the use of well-proven vessel control methods such as dynamic positioning for navigating within the marine harbor environment, and a speed- and course controller for transit between the different docks. Bumpless transfer is achieved by resetting the integrator of the receiving controller, to avoid discontinuities in the control action. Specifically, the output of two controllers are constrained to be equal at the time of transition, and the integrator state value required by the receiving controller is solved. The proposed method has been demonstrated in several simulations, taking the vessel from one dock to another in a satisfactory manner.

## 1. Introduction

Urban waterways are expected to be an integral part of the future transportation system in many cities. Urban waterways will increase the mobility for people and can be a cost-effective alternative to traditional transportation systems (Tanko and Burke, 2017). Consequently, urban passenger ferries will transport passengers on shorter pre-defined routes and can be a greener and cheaper alternative than bridges and cars. Autonomy and automatic maneuvering are key elements to make passenger ferries cost-effective, and proper path planning is necessary for safe navigation (Öztürk et al., 2022). Moreover, automating ship maneuvers and developing decision-support systems can limit the number of ship accidents by reducing the stress level of human operators (Antão and Soares, 2019). It can also be a viable alternative to move the operator to an onshore remote-control center in the future where the operator monitors several ferries simultaneously.

A passenger ferry operating between docks goes through several phases. We divide the operation into three distinct phases. *Undocking* is the first phase of a ferry operation where the ferry leaves the dock and maneuvers away from the harbor. The second phase is the *crossing* or *transit* phase where the ferry maneuvers between the harbors in open waters. The final phase is the *docking* phase where the ferry approaches the destination and tries to dock at a specific location for unloading of passengers. The phases typically have independent control strategies based on different maneuvering models due to differences in the speed regime of each phase.

The undocking phase requires a controller that pushes the ferry away from the quay with position and velocity control to leave the quay safely. This can be achieved with low-speed maneuvering using a dynamic positioning (DP) system (Fossen, 2021; Saelid et al., 1983). More advanced alternatives also exist for undocking, for example based on optimization (Wang et al., 2022; Martinsen et al., 2020; Bitar et al., 2020). The transit phase typically uses speed and course control and a line-of-sight guidance law (Fossen et al., 2003). Transit is generally conducted at higher speed and a maneuvering model that includes non-linear damping is utilized to have a model suitable for the speed regime. The docking phase needs position and heading control to maneuver precisely and is often based on path following and velocity control. Therefore, several different controllers must be combined to develop

* Corresponding author at: NTNU Centre for Autonomous Marine Operations and Systems, Department of Engineering Cybernetics, Norwegian University of Science and Technology, O. S. Bragstads plass 2D, 7491 Trondheim, Norway.

*E-mail addresses:* jens.walmsness@maritimerobotics.com (J.E. Walmsness), hakon.helgesen@ntnu.no (H.H. Helgesen), stefan.larsen@inria.fr (S. Larsen), giorgio@maritimerobotics.com (G.K.M. Kufoalor), tor.arne.johansen@ntnu.no (T.A. Johansen).

https://doi.org/10.1016/j.oceaneng.2022.113425
Received 26 August 2022; Received in revised form 26 October 2022; Accepted 11 December 2022
Available online 16 December 2022

full dock-to-dock capability. However, switching between independent controllers is not trivial and discontinuous jumps in the control action and lingering integral effects are challenges that will persist if this is done naively. This is particularly important since the different phases occur in different speed regimes that use independent maneuvering models and control strategies. Rapid accelerations and changes in the control action are uncomfortable for passengers and lead to increased fuel consumption. Moreover, the stability and maneuverability can be affected by sudden accelerations, varying water depth (Chen et al., 2021) and rapid changes in the desired states. Consequently, how to switch smoothly between different controllers is key for making automatic control systems with dock-to-dock capability. The aim of this paper is to design a robust automatic control system with dock-to-dock capability with seamless switching between the controllers in each ferry phase.

Bumpless transfer is a common term for strategies that try to switch between different controllers. Zaccarian and Teel (2002) generalizes the anti-windup approach introduced by Teel and Kapoor (1997) and applies it to the problem of bumpless transfer. By using supervisory switching (Nguyen et al., 2008), all the controllers, even the unconnected ones, are fed "fictitious" dynamics, letting them develop as if they were connected to the plant. Thus, when switching controllers, the plant's current state smoothly converges to the fictitious state without any jumps in desired control action, enabling smooth transitions between controllers. A downside is that every controller is running at the same time through feedback of the control signal. Consequently, this may be computationally expensive for certain systems. Lourenco and Lemos (2006) also uses a supervisory system, but bumpless transfer is achieved through a common integrator. By connecting all controllers to a common integrator, continuity in the control signal is ensured.

Another solution to the bumpless transfer problem is through state resetting. Kinnaert et al. (2009) considers a multi-controller scheme using a supervisory framework. When switching between two controllers, the states of the new controller are initialized as if it had been the previously active controller. To achieve this, a coherent reference signal is necessary, which can be calculated by means of controller inversion (Pasamontes et al., 2010). Consequently, a prerequisite for this method is a state-space representation of both controllers. Pasamontes et al. (2011) proposes a similar technique, however, it requires less information on past states and also facilitates transitioning between control regimes featuring both feedback- and feedforward controllers. However, both of these techniques require coherent reference signals, which can be a challenge when several different guidance laws are involved.

This paper investigates how an automatic dock-to-dock control system can be designed with independent controllers for each phase. A DP controller is used for undocking at low speed together with a guidance scheme that ensures that the ferry leaves the quay safely. Bumpless transfer is used to switch between the undocking controller and the transit controller. The transit controller is based on speed and course controllers where a line-of-sight guidance law is used to generate the desired course angle to move between the harbors at a desired cruise speed. Bumpless transfer is used to transition from the transit phase to the docking phase. The docking control system is based on a DP system with low-speed assumptions and a third-order reference model.

The main contribution of this paper is the bumpless transfer design which ensures that the switching between phases can occur at any point in time. A zero-velocity criterion (Bitar et al., 2021) is typically used in existing literature to change between different controllers on surface vessels. This is avoided here and improves the flexibility and efficiency of the dock-to-dock system. A supervisor is designed to maintain the high-level decision making and initialize switching between the phases. The automatic dock-to-dock system is modular and the low-level controllers in each phase can be replaced without affecting other parts of the system. The method has a small computational footprint and is suitable for both large boats and smaller autonomous vessels.

The rest of this paper is organized in six sections. Section 2 introduces preliminaries and modeling of marine surface vessels. The guidance laws and low-level controllers used for simulations are presented in Section 4, including the proposed bumpless transfer solution. Section 3 describes the dock-to-dock architecture. Section 5 present the simulation results from the bumpless transfer and dock-to-dock tests. Section 6 concludes the paper and proposes suggestions for future work.

## 2. Modeling of marine surface vessels

This section presents the mathematical model used to model the ferry in the dock-to-dock scenario.

### 2.1. Reference frames and generalized coordinates

When describing the motion of a surface vessel in a local area, two different reference frames are needed:

- *The North-East-Down (NED) reference frame* is a tangent plane fixed on the Earth's surface, used for local navigation. It is expressed as $\{n\} = (x_n, y_n, z_n)$, where the $x_n$ axis points towards the true geographic north, $y_n$ towards the east, and the $z_n$ axis points downwards, normal to the Earth's surface.
- *The BODY frame* is a reference frame fixed to the marine craft, and it is defined as $\{b\} = (x_b, y_b, z_b)$. The longitudinal axis $x_b$ goes from aft to fore, the transversal axis $y_b$ is directed towards the starboard, and the normal axis $z_b$ goes from the deck to the keel. Typically, the origin of the body frame is often placed at the vessel's nominal center of gravity.

One can move between these frames by means of a rotation matrix where attitude is parameterized through the heading angle when horizontal motion in the plane is considered

$$\dot{\boldsymbol{\eta}} = \boldsymbol{R}_b^n(\psi)\boldsymbol{\nu} \quad \text{or} \quad \begin{bmatrix} \dot{x} \\ \dot{y} \\ \dot{\psi} \end{bmatrix} = \begin{bmatrix} \cos\psi & -\sin\psi & 0 \\ \sin\psi & \cos\psi & 0 \\ 0 & 0 & 1 \end{bmatrix} \begin{bmatrix} u \\ v \\ r \end{bmatrix} \tag{1}$$

where the generalized position and velocity vectors are $\boldsymbol{\eta} = [x, y, \psi]^\top$ and $\boldsymbol{\nu} = [u, v, r]^\top$, given in {n} and {b}, respectively, where $\psi$ is the yaw angle and $r$ is its angular rate. $\boldsymbol{R}_b^n(\psi)$ is a principle rotation around the $z$-axis (yaw), rotating a vector from {b} to {n}.

### 2.2. Ship modeling

A fully actuated 3 DOF nonlinear maneuvering model is chosen for simulations in this work

$$\dot{\boldsymbol{\eta}} = \boldsymbol{R}_b^n(\psi)\boldsymbol{\nu} \tag{2a}$$

$$\boldsymbol{M}\dot{\boldsymbol{\nu}}_r + \boldsymbol{N}(\boldsymbol{\nu}_r)\boldsymbol{\nu}_r = \boldsymbol{\tau} + \boldsymbol{\tau}_{\text{wind}} + \boldsymbol{\tau}_{\text{wave}} \tag{2b}$$

where $\boldsymbol{M} = \boldsymbol{M}_{\text{RB}} + \boldsymbol{M}_A$ is the total mass matrix, consisting of a rigid-body and an added mass matrix due to hydrodynamic forces. $\boldsymbol{N}(\boldsymbol{\nu}_r) = \boldsymbol{C}_{\text{RB}}(\boldsymbol{\nu}_r) + \boldsymbol{C}_A(\boldsymbol{\nu}_r) + \boldsymbol{D}$ is a collective term with Coriolis and centripetal terms together with linear hydrodynamic damping (Fossen, 2021, Chapter 6). Note that $\boldsymbol{\nu}_r$ denotes the relative velocity vector $\boldsymbol{\nu}_r = \boldsymbol{\nu} - \boldsymbol{\nu}_c$, where $\boldsymbol{\nu}_c$ is the generalized ocean current velocity vector represented in the {b} frame. $\boldsymbol{\tau}_{\text{wind}}$ and $\boldsymbol{\tau}_{\text{wave}}$ are the wind- and wave-induced forces, respectively, while $\boldsymbol{\tau}$ are thruster control forces. It is assumed that the vessel is sufficiently damped in roll. Moreover, surge is decoupled from sway and yaw due to port-starboard symmetry, thus the system matrices take the following form

$$\boldsymbol{M} = \begin{bmatrix} m_{11} & 0 & 0 \\ 0 & m_{22} & m_{23} \\ 0 & m_{32} & m_{33} \end{bmatrix}, \quad \boldsymbol{D} = \begin{bmatrix} d_{11} & 0 & 0 \\ 0 & d_{22} & d_{23} \\ 0 & d_{32} & d_{33} \end{bmatrix}$$

$$\boldsymbol{C} = \begin{bmatrix} 0 & 0 & c_{13}(\boldsymbol{\nu}_r) \\ 0 & 0 & c_{23}(\boldsymbol{\nu}_r) \\ c_{31}(\boldsymbol{\nu}_r) & c_{32}(\boldsymbol{\nu}_r) & 0 \end{bmatrix}$$

### 2.3. Wind disturbance

Wind can be divided into two components: a steady average component and a fluctuating gust component. From (2), $\boldsymbol{\tau}_{\text{wind}}$ can be modeled in 3 DOF for a moving vessel as (Fossen, 2021, Chapter 10)

$$\boldsymbol{\tau}_{\text{wind}} = \frac{1}{2}\rho_a V_{rw}^2 \begin{bmatrix} C_X(\gamma_{rw})A_{F_w} \\ C_Y(\gamma_{rw})A_{L_w} \\ C_N(\gamma_{rw})A_{F_w}L_{oa} \end{bmatrix} \tag{3}$$

where $\rho_a$ is the air density, $A_{F_w}$ and $A_{L_w}$ are the frontal and lateral projected areas, and $L_{oa}$ is the overall length of the vessel. $C_X, C_Y, C_N$ are wind coefficients that can be calculated from equations given by Blendermann (1994). For a moving vessel, the relative wind velocity $V_{rw}$, and angle of attack $\gamma_{rw}$ are used:

$$V_{rw} = \sqrt{u_{rw}^2 + v_{rw}^2} \tag{4}$$

$$\gamma_{rw} = -\text{atan2}(v_{rw}, u_{rw}) \tag{5}$$

where $u_{rw}$ and $v_{rw}$ are the relative wind directions in surge and sway, respectively.

## 3. Dock-to-dock architecture

The proposed method divides the dock-to-dock scheme into three modes: UNDOCKING, TRANSIT, and DOCKING. The UNDOCKING mode uses a standard reference filter and DP controller as described in Sections 4.1.1 and 4.2.1. The DOCKING mode uses the same controller and filter, but they are modified in the later stages of berthing. The TRANSIT mode uses the line-of-sight guidance algorithm described in Section 4.1.2, and the speed- and course controllers from Section 4.2.2. Motion in sway is not controlled directly in the transit phase and this is common in transit and higher speed domains. Additionally, the bumpless transfer solution from Section 4.3 handles the transitions between the different modes, ensuring smooth transitions when switching between the different control regimes. The transitions themselves are handled by the use of waypoints. A mechanism to detect when the vessel is sufficiently close to the waypoint is necessary. This can be done through a circle of acceptance, or the more versatile ellipse of acceptance.

$$\frac{((y_c - y^n)\cos\varphi - (x_c - x^n)\sin\varphi)^2}{a^2} + \frac{((y_c - y^n)\sin\varphi - (x_c - x^n)\cos\varphi)^2}{b^2} \leq 1 \tag{6}$$

where $(x_c, y_c)$ is the center of the ellipse, $(x^n, y^n)$ is the craft's position in {n}, and $a$ and $b$ are the lengths of the semi-major- and semi-minor axis, respectively. Additionally, the ellipse can be rotated by an angle $\varphi \in [-180°, 180°]$, where 0° is defined as north and 90° is east. This structure can be implemented as a state machine, depicted in Fig. 1. The UNDOCKING mode begins by moving the vessel in a straight line away from the quay with constant heading. This is the first UNDOCKING waypoint, and is meant to safely bring the vessel away from the quay structure without rotating. Following, the vessel maneuvers to the launch waypoint, which has a larger ellipse of acceptance. This is in order to let the vessel carry its speed before transitioning to TRANSIT, as normally a DP controller will slow down and stop once it reaches its waypoint. Transitioning to the TRANSIT mode, the reference filter and DP controller go to idle, and the line-of-sight (LOS) and transit controllers are initialized. Additionally, the bumpless transfer functionality described in Section 4.3 triggers as the vessel switches modes. Note that during transitions it is preferable (although not necessary with bumpless transfer) to match the vessel's speed to the new controller's reference speed, in order to avoid reference misalignment. In TRANSIT, the vessel iterates through its waypoints until it reaches the final approach waypoint. Here, the mode switches from TRANSIT to DOCKING and the reference filter and DP controller take over while bumpless transfer ensures smoothness. In the final DOCKING mode, the algorithm proposed by Knudsen (2021) and further modified by Larsen (2022), guides the vessel to its berthing location. Note that the final *docking* mode uses waypoints to approach the quay, signified by the *quay_wp_reached* flag. Alternatively, this can be achieved through quay contact detection (Helgesen et al., 2022) or berthing state estimation (Hu et al., 2022) for improved efficiency and robustness.

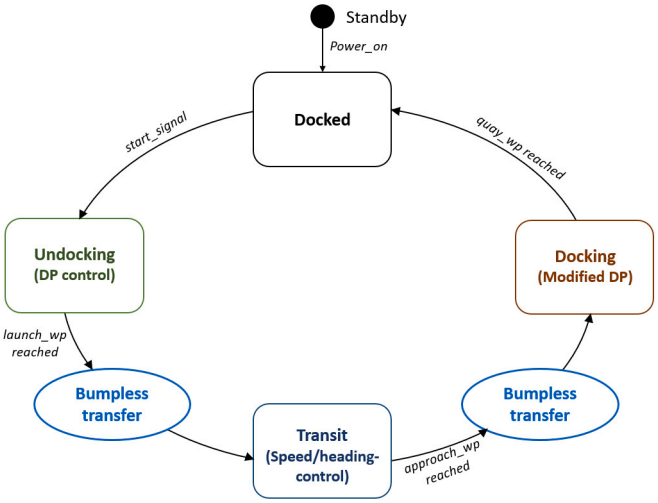


**Fig. 1.** The dock-to-dock method expressed as a state machine. Note the intermediate bumpless transfer nodes between the operational modes.

## 4. Guidance and control

This section describes the guidance schemes and the controllers used in the dock-to-dock scenario. In addition, a bumpless transfer algorithm is presented to switch between the controllers in each phase.

### 4.1. Guidance

Two separate guidance laws are used for simulations, a reference filter during low-speed maneuvering with DP, and a line-of-sight (LOS) guidance scheme during transit operations.

#### 4.1.1. Reference filter

The reference filter generates smooth trajectories and is motivated by the dynamics of a mass–spring–damper system (Fossen, 2021). It can be expressed as

$$\boldsymbol{\eta}_d^{(3)} + (2\boldsymbol{\Delta} + \boldsymbol{I})\boldsymbol{\Omega}\ddot{\boldsymbol{\eta}}_d + (2\boldsymbol{\Delta} + \boldsymbol{I})\boldsymbol{\Omega}^2\dot{\boldsymbol{\eta}}_d + \boldsymbol{\Omega}^3\boldsymbol{\eta}_d = \boldsymbol{\Omega}^3\boldsymbol{r}^n \tag{7}$$

where $\boldsymbol{\eta}_d$ is the desired position vector, $\boldsymbol{r}^n$ is the reference position vector, and the diagonal matrices $\boldsymbol{\Delta}$ and $\boldsymbol{\Omega}$ are the relative damping ratio matrix and natural frequency matrix, respectively. The filter is of third order to ensure smooth signals to the tracking control system. Additionally, saturation elements are added for velocity and acceleration to avoid unreasonable changes in the reference signals. This ensures that the generated references are physically feasible for the vessel to follow.

#### 4.1.2. Line-of-sight guidance

During transit, where the vessel is traveling long distances across open waters, path fallowing is the common guidance method. Path-following, contrary to trajectory tracking, does not have any temporal specifications, only concerning itself with maintaining the desired path. This path can be generated by the use of waypoints:

$$\boldsymbol{\eta}_{\text{WP}} = [x^n, y^n, U]^\top \tag{8}$$

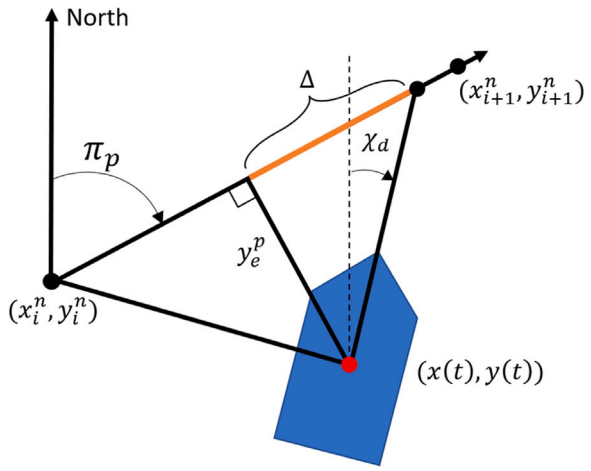


**Fig. 2.** Figure showing the LOS method and relevant variables.

where $U$ is the desired forward speed and $(x^n, y^n)$ is the desired position of a waypoint. For harbor maneuvering using dynamic positioning, $\psi$ replaces $U$, as one wishes to control the heading angle of the vessel and the horizontal position. The LOS guidance law forms a triangle from three points: a reference point (the previous waypoint), a target point (the next waypoint), and the current position of the vessel. See Fig. 2 for a sketch of the LOS method. The path generated by the reference point and the target point is called the LOS path. The distance from the LOS path to the marine craft is the cross-track error, $y_e^p$. The goal of the LOS guidance law is to make this cross-track error go to zero. It does so by aiming towards a point on the LOS path, the lookahead distance $\Delta$. The cross-track error can be derived from the triangle formed by the three points

$$y_e^p = -(x(t) - x_i^n)\sin(\pi_p) + (y(t) - y_i^n)\cos(\pi_p) \tag{9}$$

where $x(t)$ and $y(t)$ are the current position in NED, and $x_i^n$ and $y_i^n$ are the coordinates of the previous waypoint. $\pi_p$ is the path-tangential angle and is given by

$$\pi_p = \text{atan2}(y_{i+1}^n - y_i^n, x_{i+1}^n - x_i^n) \tag{10}$$

with the subscript $i$ and $i+1$ denoting the previous and current waypoint. Finally, the desired course angle can be calculated as

$$\chi_d = \pi_p - \tan^{-1}\left(\frac{y_e^p}{\Delta}\right) \tag{11}$$

The guidance controller also features an adaptive lookahead distance, based on Lekkas and Fossen (2012):

$$\Delta = (\Delta_{\max} - \Delta_{\min})e^{-\gamma|y_e^p|} + \Delta_{\min} \tag{12}$$

where $\Delta_{\max}$, $\Delta_{\min}$ are the maximum and minimum lookahead distances respectively, and $\gamma$ is the convergence rate. A lookahead distance following this law will be small if the vessel is far from the desired path and large if it is close to the desired path. This ensures that the vessel steers towards the desired path fairly aggressively if it is far away and avoids oscillations when close.

### 4.2. Control

Two different low-level controllers are used: a DP controller during UNDOCKING and DOCKING, and a speed and course controller during TRANSIT.

#### 4.2.1. Dynamic positioning controller

A common design choice for the DP controller is the linear time-varying model, based on the nonlinear 3 DOF model in (2). The linear time-varying model is expressed as

$$\dot{\boldsymbol{\eta}} = \boldsymbol{R}(t)\boldsymbol{\nu} \tag{13a}$$

$$\boldsymbol{M}\dot{\boldsymbol{\nu}} + \boldsymbol{D}\boldsymbol{\nu} = \boldsymbol{R}^\top(t)\boldsymbol{b} + \boldsymbol{\tau} + \boldsymbol{\tau}_{\text{wind}} \tag{13b}$$

$$\dot{\boldsymbol{b}} = \boldsymbol{0} \tag{13c}$$

where $\boldsymbol{b}$ is a slowly-varying bias vector representing ocean currents and other unmodeled effects. Note that of the collective term $\boldsymbol{N}(\boldsymbol{\nu}_r) = \boldsymbol{C}_{\text{RB}}(\boldsymbol{\nu}_r) + \boldsymbol{C}_A(\boldsymbol{\nu}_r) + \boldsymbol{D}$ in (2), only the damping matrix $\boldsymbol{D}$ remains in the DP model (13b) in addition to the bias $\boldsymbol{b}$. For low-speed applications such as harbor maneuvering, linear damping is a good assumption (Fossen, 2021). The quadratic velocity terms from the Coriolis matrix can be neglected at low speed if the ocean current is compensated for by integral action, as is done with the addition of the bias term $\boldsymbol{b}$. Note that $\tau_{\text{wave}}$ from (2) is omitted. Commonly, DP is used for offshore vessels with the goal of maintaining a fixed position and heading, however, in this paper it is used for low-speed maneuvering in marine harbor environments. Consequently, it is assumed that the waves are of a smaller magnitude and are filtered by the bias term $\boldsymbol{b}$. The generalized position $\boldsymbol{\eta}$ can be measured if the vessel is equipped with a global navigation satellite system (GNSS) receiver and a heading reference system. This allows for the kinematic nonlinearity due to the rotation matrix to be removed by assuming that $\boldsymbol{R}(t) := \boldsymbol{R}_{z,\psi}(\psi(t))$ is known for all $t \geq 0$.

The control system can be designed as a multiple-input and multiple-output (MIMO) nonlinear PID controller:

$$\boldsymbol{\tau} = -\hat{\boldsymbol{\tau}}_{\text{wind}} + \boldsymbol{R}^\top(t)\boldsymbol{\tau}_{\text{PID}} \tag{14}$$

where $\hat{\boldsymbol{\tau}}_{\text{wind}}$ is an estimate of the generalized wind forces using a feedforward term

$$\hat{\boldsymbol{\tau}}_{\text{wind}} = k_{\text{FF, vel}}\hat{\boldsymbol{\tau}}_{\text{FF, vel}} \tag{15}$$

with measured wind velocity feedforward to better compensate for slowly-varying wind forces. $\boldsymbol{\tau}_{\text{PID}}$ is a standard controller expressed in {n}:

$$\boldsymbol{\tau}_{\text{PID}} = -\boldsymbol{K}_p\tilde{\boldsymbol{\eta}} - \boldsymbol{K}_d\dot{\tilde{\boldsymbol{\eta}}} - \boldsymbol{K}_i\int_0^t \tilde{\boldsymbol{\eta}}(\tau)\mathrm{d}\tau \tag{16}$$

with $\tilde{\boldsymbol{\eta}} := \boldsymbol{\eta} - \boldsymbol{\eta}_{\text{ref}}$ being the error in the generalized position. The DP controller also features an anti-windup scheme, saturating the integral action to a given threshold $\boldsymbol{\tau}_{\text{windup}}$. Defining the integrator as $\boldsymbol{Z} = \int_0^t \tilde{\boldsymbol{\eta}}(\tau)\mathrm{d}\tau$, the saturation can be implemented as

$$\boldsymbol{Z} = \min\{\boldsymbol{\tau}_{\text{windup}}, \max\{-\boldsymbol{\tau}_{\text{windup}}, \boldsymbol{Z}\}\} \tag{17}$$

limiting the integrator to the accepted values

$$\boldsymbol{Z} \in [-\boldsymbol{\tau}_{\text{windup}}, \boldsymbol{\tau}_{\text{windup}}] \tag{18}$$

#### 4.2.2. Speed and course controller

The transit controller consists of a speed and course controller, following a path generated by the LOS guidance law. The desired speed is specified in the waypoint as in (8), and a reference model is used to avoid steps in this signal. In surge, it takes the form of a second-order low-pass (LP) filter

$$\frac{u_d}{u_{\text{ref}}}(s) = \frac{\omega_{n,u}^2}{s^2 + 2\zeta_u\omega_{n,u}s + \omega_{n,u}^2} \tag{19}$$

where $\omega_{n,u}$ is the natural frequency, and $\zeta_u$ is the relative damping ratio. Since the reference model is of second order, a step in the command $u_{\text{ref}}$ will give a step in the jerk $\dddot{u}_d$, while the acceleration $\ddot{u}_d$ and velocity $u_d$ will be low-pass filtered and therefore be continuous signals. Eq. (19) is converted to a state-space representation and will generate the desired surge speed $u_d$ and surge acceleration $\dot{u}_d$. This is then fed to a PI-controller to calculate the desired force in surge $X$

$$X = d_{11}u_d + m_{11}\dot{u}_d - K_p\tilde{u} - K_i\int_0^t \tilde{u}\mathrm{d}\tau \tag{20}$$

where $\tilde{u} = u - u_d$ is the tracking error in surge. The first two terms are for reference feedforward, $d_{11}$ and $m_{11}$ being the damping- and mass

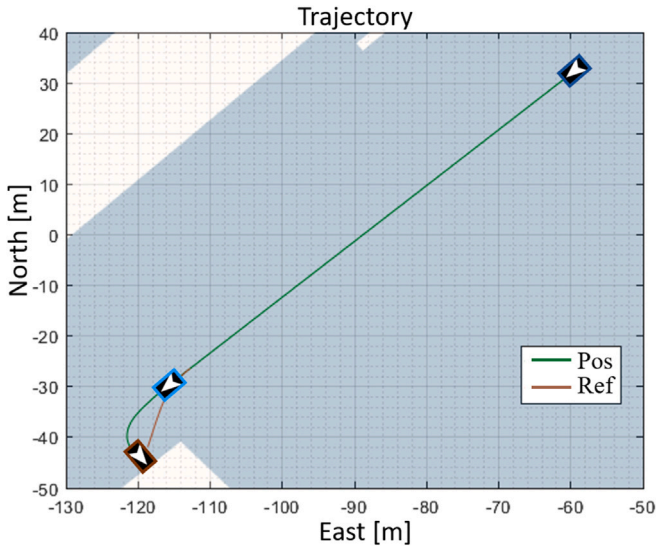


**Fig. 3.** Plot of the trajectory from a TRANSIT to DOCKING test with an overlay from the mA simulator map and the pose of the vessel at the waypoints listed in Table 1. The vessel starts in TRANSIT (dark blue), then transitions (light blue) to DOCKING (brown). (For interpretation of the references to color in this figure legend, the reader is referred to the web version of this article.)

element in surge, respectively. The PI-controller is designed with the 3 DOF nonlinear maneuvering model (2) in mind. The objective is to cancel out the system matrices with the reference feedforward terms and use the PI-terms to drive the states towards the desired reference value.

A pole-placement algorithm can find the values for $K_p$ and $K_i$. By specifying the tuning parameters, bandwidth $\omega_b$ and relative damping ratio $\zeta$, the natural frequency $\omega_n$ can be computed as

$$\omega_n = \frac{1}{\sqrt{1 - 2\zeta^2 + \sqrt{4\zeta^4 - 4\zeta^2 + 2}}}\omega_b \tag{21}$$

Consequently, the gains are given by

$$K_p = m_{11}\omega_n^2 \tag{22}$$

$$K_i = \frac{\omega_n}{10}K_p \tag{23}$$

The factor $\frac{1}{10}$ is given as a rule-of-thumb by Fossen (2021, Chapter 15)

$$\frac{K_i}{K_p} \approx \frac{\omega_n}{10} \tag{24}$$

Preferably one wants a small value for the integrator gain, as it introduces lags and phase shifts. This rule-of-thumb guarantees that the integrator is ten times slower than the natural frequency $\omega_n$.

Similarly to the surge controller, a reference filter is implemented in course to avoid steps in the control input.

$$\frac{\chi_d}{\chi_{\text{ref}}}(s) = \frac{\omega_{n,\chi}^3}{(s + \omega_{n,\chi})(s^2 + 2\zeta_\chi\omega_{n,\chi}s + \omega_{n,\chi}^2)} \tag{25}$$

Note that the course reference model is an LP filter cascaded with a mass–spring–damper system. Since the position is one order lower than velocity, a third-order reference model is needed to filter steps in $\chi_{\text{ref}}$. This ensures continuous signals for the angular acceleration $\dot{\chi}_d$, angular velocity $\dot{\chi}_d$, and the course angle $\chi_d$. Again, this is converted to a state-space representation, yielding the desired course angle $\chi_d$, angular velocity $r_d$, and angular acceleration $\dot{r}_d$. Note that the crab angle is assumed slowly-varying so that the course rate $\dot{\chi}$ is approximated as the yaw rate $\dot{r}$. To get the desired control action in yaw $N$, a PID controller is used

$$N = m_{33}\dot{r}_d + c_{31}u_d + d_{33}r_d - K_p\tilde{\chi} - K_d\tilde{r} - K_i\int_0^t \tilde{\chi}(\tau)\mathrm{d}\tau \tag{26}$$

The first three terms are for reference feedforward, where $m_{33}$, $c_{31}$, $d_{33}$ are elements from the mass, Coriolis, and damping matrices respectively. $\tilde{\chi} = \chi - \chi_d$ is the tracking error in course angle, and $\tilde{r} = r - r_d$ is the error in the yaw (or course) rate.

The Nomoto model is a common choice for model-based course autopilots for marine crafts (Nomoto et al., 1956). It is a simplified model for finding gains, as it directly relates the course angle $\chi$ to the rudder displacement $\delta$ as

$$\frac{\chi}{\delta}(s) = \frac{K}{s(Ts + 1)} \tag{27}$$

where its time-domain representation is

$$T\ddot{\chi} + \dot{\chi} = K\delta \tag{28}$$

This is the first-order Nomoto model, where $T$ is the Nomoto time constant, and $K$ is the rudder (Nomoto) gain. Using this model, the PID controller gains can be expressed as follows (Fossen, 2021, Chapter 15.3.4)

$$K_p = \omega_n^2\frac{T}{K}, \quad K_d = \frac{2\zeta\omega_n T - 1}{K}, \quad K_i = \omega_n^3\frac{T}{10K} \tag{29}$$

where $\omega_n$ is given by Eq. (21), and the bandwidth $\omega_b$ and relative damping ratio $\zeta$ are design parameters. $T$ and $K$ can be identified by observing a step response from the helm or a more advanced maneuvering test.

### 4.3. Bumpless transfer

To ensure smooth transitions when switching between controllers, bumpless transfer functionality is necessary. In a general case with two controllers

$$U_1 = f_1(Y, Z_1) \tag{30a}$$

$$U_2 = f_2(Y, Z_2) \tag{30b}$$

where $Z_1$ and $Z_2$ are internal states and $Y$ are inputs, when switching from $U_1$ to $U_2$ one wants $U_1 = U_2$ to ensure continuity. This is achieved by solving the following equation for $Z_2$ (Aström and Hägglund, 1995, Chapter 3)

$$U_1 = f_2(Y, Z_2) \tag{31}$$

Typically, $Z_1$ and $Z_2$ are integrators and $\dim(Z_2) = \dim(U_1)$, so the problem has a unique solution. If $\dim(Z_2) < \dim(U_1)$, then continuity can only be maintained in some degrees of freedom. In the case of the DP controller and the transit controller described in Section 4.2, (30) takes the following form:

$$U_1 = \boldsymbol{\tau}_{\text{PID}} = \left[X_{\text{DP}},\ Y_{\text{DP}},\ N_{\text{DP}}\right]^\top \tag{32a}$$

$$U_2 = \boldsymbol{\tau}_{\text{Transit}} = \left[X_{\text{Transit}},\ N_{\text{Transit}}\right]^\top \tag{32b}$$

Where $\boldsymbol{\tau}_{\text{PID}}$ is defined in (16), and $X_{\text{Transit}}$ and $N_{\text{Transit}}$ are (20) and (26), respectively. From (32) it is observed that $\dim(U_1) = 3$ and $\dim(U_2) = 2$. Similarly, while DP has an integrator in all the 3 DOF, the transit controller only controls surge and yaw, thus $\dim(Z_1) = 3$ and $\dim(Z_2) = 2$. Since $\dim(Z_2) < \dim(U_1)$, only surge and yaw can maintain continuity in the control action when going from DP to transit. Conversely, going from transit to DP allows a continuous control action in all DOF. Moreover, it can be noted that the states of the two controllers are also different. This is a challenging problem, and unlike other solutions from literature this method does not require coherent reference signals in order to ensure continuity (Kinnaert et al., 2009; Pasamontes et al., 2011), nor does it require any state restrictions (Bitar et al., 2021).

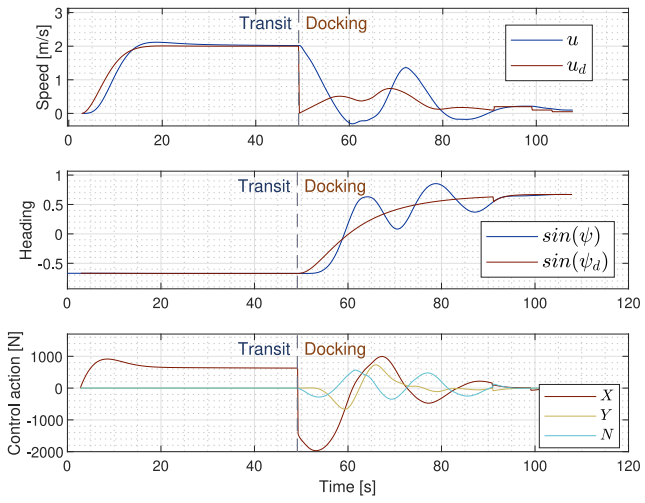


(a) 2.0 m/s entry speed without bumpless transfer.

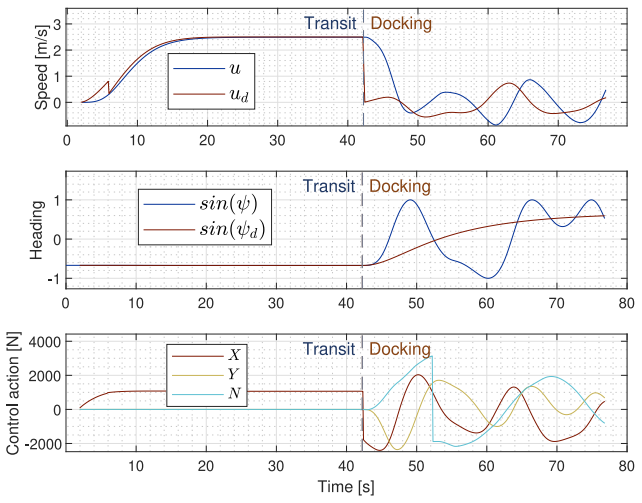


(b) 2.5 m/s entry speed without bumpless transfer.

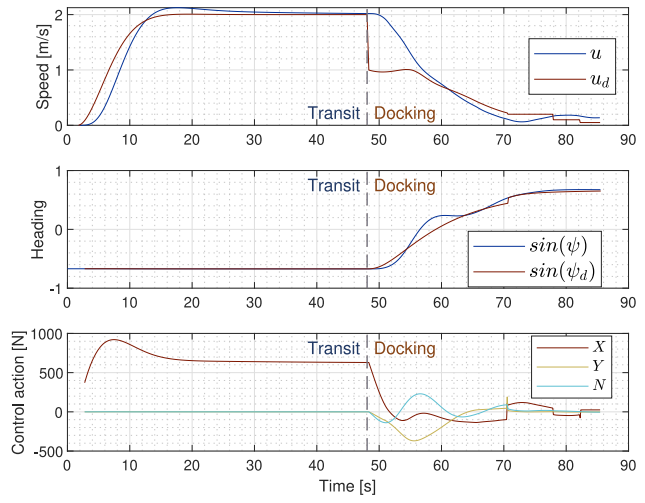


(c) 2.0 m/s entry speed with bumpless transfer.

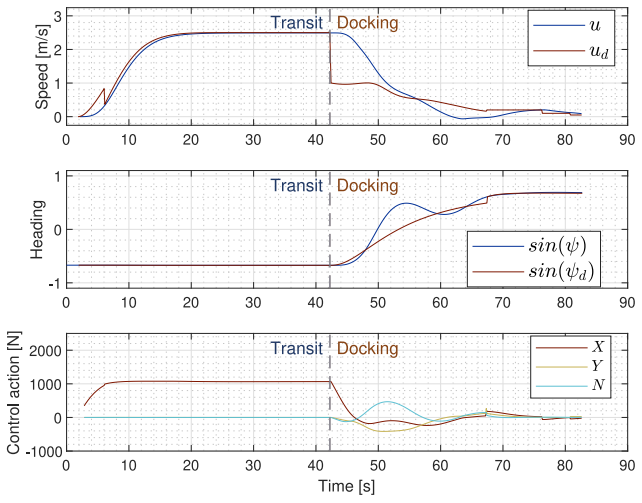


(d) 2.5 m/s entry speed with bumpless transfer.

**Fig. 4.** Plots of the surge speed, heading, and control action for the different TRANSIT to DOCKING tests.

Starting with the DP to transit transition, (30) takes the following form in surge:

$$X_{\text{DP}} = -K_p\tilde{x} - K_d\dot{\tilde{x}} - K_i\int_0^t \tilde{x}(\tau)\mathrm{d}\tau \tag{33a}$$

$$X_{\text{Transit}} = d_{11}u_d + m_{11}\dot{u}_d - K_p\tilde{u} - K_i\int_0^t \tilde{u}\mathrm{d}\tau \tag{33b}$$

Defining the reference feedforward term $\tau_{\text{FF, surge}} = d_{11}u_d + m_{11}\dot{u}_d$ and identifying the integrator $Z_{surge} = \int_0^t \tilde{u}\mathrm{d}\tau$, gives the following when inserting in (31):

$$X_{\text{DP}} = \tau_{\text{FF, surge}} - K_p\tilde{u} - K_i Z_{surge} \tag{34}$$

Solving for the integrator $Z_{surge}$ yields the value needed to ensure $U_1 = U_2$:

$$Z_{surge} = K_i^{-1}\left(\tau_{\text{FF, surge}} - K_p\tilde{u} - X_{\text{DP}}\right) \tag{35}$$

This will cause a jump in the integrator state, but the desired control action will remain continuous during the transition. The yaw case can be solved similarly. Recall that the course controller is given as:

$$N_{\text{Transit}} = m_{33}\dot{r}_d + c_{31}u_d + d_{33}r_d - K_p\tilde{\chi} - K_d\tilde{r} - K_i\int_0^t \tilde{\chi}(\tau)\mathrm{d}\tau \tag{36}$$

Again, defining the feedforward term $\tau_{\text{FF, yaw}} = m_{33}\dot{r}_d + c_{31}u_d + d_{33}r_d$ and the integrator as $Z_{yaw} = \int_0^t \tilde{\chi}(\tau)\mathrm{d}\tau$, this can be inserted in (31) and solved for $Z_{yaw}$

$$Z_{yaw} = K_i^{-1}\left(\tau_{\text{FF, yaw}} - K_p\tilde{u} - K_d\tilde{r} - N_{\text{DP}}\right) \tag{37}$$

ensuring continuity in the desired control action.

When transitioning from the transit controller to DP (docking), the equations are reversed. As the dynamic positioning control system is expressed in NED, the equations differ slightly due to the rotation matrix $\boldsymbol{R}$. Recall the DP controller system equation

$$\boldsymbol{\tau} = -\hat{\boldsymbol{\tau}}_{\text{wind}} + \boldsymbol{R}^{\top}(t)\boldsymbol{\tau}_{\text{PID}}$$

where the left-hand side $\boldsymbol{\tau}$ will be the control action from the transit controller $\boldsymbol{\tau}_{\text{transit}}$ and $\boldsymbol{\tau}_{\text{PID}}$ is given in (16). Following the previous notation, it can be noted that $\boldsymbol{\tau}_{\text{FF}} = -\hat{\boldsymbol{\tau}}_{\text{wind}}$. Inserting (16) and writing it on the form of (31) yields

$$\boldsymbol{\tau}_{\text{Transit}} = \boldsymbol{\tau}_{\text{FF}} + \boldsymbol{R}^{\top}\left[-\boldsymbol{K}_p\tilde{\boldsymbol{\eta}} - \boldsymbol{K}_d\dot{\tilde{\boldsymbol{\eta}}} - \boldsymbol{K}_i\int_0^t \tilde{\boldsymbol{\eta}}(\tau)\mathrm{d}\tau\right] \tag{38}$$

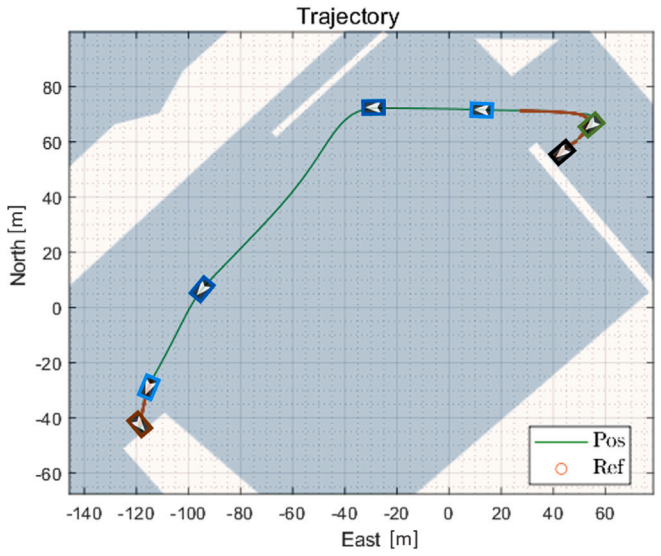


**Fig. 5.** Plot of the trajectory from a dock-to-dock test overlayed with the mA simulator map and the pose of the vessel at the waypoints listed in Table 4. It is taken from a test with bumpless transfer and without any wind. From being docked (black), the vessel begins UNDOCKING (green), goes to TRANSIT (dark blue), then transitions (light blue) to DOCKING (brown). (For interpretation of the references to color in this figure legend, the reader is referred to the web version of this article.)

where we identify the integrator term as $\boldsymbol{Z} = \int_0^t \tilde{\boldsymbol{\eta}}(\tau)\mathrm{d}\tau$. Finally, solving for $\boldsymbol{Z}$ gives the bumpless transfer equation from transit to docking

$$\boldsymbol{Z} = \boldsymbol{K}_i^{-1}\left[-\boldsymbol{K}_p\tilde{\boldsymbol{\eta}} - \boldsymbol{K}_d\dot{\tilde{\boldsymbol{\eta}}} - \boldsymbol{R}\left(\boldsymbol{\tau}_{\text{transit}} - \boldsymbol{\tau}_{\text{FF}}\right)\right] \tag{39}$$

where $\boldsymbol{Z} = [Z_{\text{surge}}, Z_{\text{sway}}, Z_{\text{yaw}}]^\top$. $Z_{\text{sway}}$ is the sway integrator. This method ensures there are no jumps in the desired control action when transitioning from the transit controller to the DP controller.

## 5. Results

This section covers the experimental setup used for testing and presents the results. The presented results are a subset of a wide array of testing, and showcase the most important scenarios which aim to demonstrate both the strengths and weaknesses of the dock-to-dock and bumpless transfer methods. The results in this paper are split into two parts: a transit to docking case and a dock-to-dock case.

### 5.1. Experimental setup

The tests are performed on the milliAmpere (mA) simulator, a prototype vessel at NTNU to further advance autonomous ferries. The simulator is described more closely in Pedersen (2019) and the numerical values in the simulator are based on the actual ferry. Moreover, a heading autopilot with crab-angle compensation is used in these experiments, which is interchangeable with a course controller. It should be noted that the performance of the DP and transit controllers themselves is not the focus of these results. If they are studied, it will be in the moments after a transition, investigating the effects of bumpless transfer on the independent controllers.

### 5.2. Transit to docking task

The bumpless transfer functionality will be investigated in detail with the vessel going from TRANSIT to DOCKING. Generally, this transition is the most challenging one, as the vessel has to reduce its speed as it approaches the quay structure while changing from control in 2 DOF (course and speed) to 3 DOF control in DP. Two test cases will be presented: one where the vessel transitions from TRANSIT to DOCKING with an entry speed of 2.0 m/s, and another at 2.5 m/s. The first two tests are without bumpless transfer, setting a benchmark for a comparison with two identical tests with bumpless transfer functionality. The test route is depicted in Fig. 3, following the waypoints given in Table 1. The two docking waypoints are the berthing and quay waypoints, respectively, for more details see Knudsen (2021), Larsen (2022).

**Table 1**
Table showing the waypoints used in the TRANSIT and DOCKING modes. The initial state of the vessel is [32, −61, −138°].

| Transit [North, East , $U$] | Docking [North, East , $\psi$] |
|---|---|
| [−30.6, −116.6, 2.5] | [−45.5, −119.5, 138.0] |
| | [−47.0, −118.0, 138.0] |

**Table 2**
Table of the minimum- and maximum values of the heading error, as well as the RMSE. All values are given in degrees.

| | Min value | Max value | RMSE |
|---|---|---|---|
| **2.0 m/s entry speed** | | | |
| Without bumpless | −28.5 | 20.3 | 9.6 |
| With bumpless | −12.8 | 6.1 | 3.2 |
| **2.5 m/s entry speed** | | | |
| Without bumpless (Failed) | – | – | – |
| With bumpless | −27.2 | 5.0 | 7.7 |

**Table 3**
Table of the minimum- and maximum values of the surge velocity error, as well as the RMSE. All values are given in m/s.

| | Min value | Max value | RMSE |
|---|---|---|---|
| **2.0 m/s entry speed** | | | |
| Without bumpless | −0.75 | 2.01 | 0.43 |
| With bumpless | −0.47 | 1.04 | 0.27 |
| **2.5 m/s entry speed** | | | |
| Without bumpless (Failed) | – | – | – |
| With bumpless | −0.50 | 1.52 | 0.40 |

Fig. 4 shows the vessel's surge speed, heading, and control action for the various TRANSIT to DOCKING tests. Tables 2 and 3 show the minimum and maximum error values and the root-mean-squared deviation (RMSE) for the heading and surge velocity respectively. Comparing Figs. 4(a) and 4(c), the effects of bumpless transfer are apparent. Studying the control action, the surge force in particular, the discontinuity is replaced by a smooth descent in surge force following the transition. Also note the significant reduction in the surge force with bumpless transfer functionality, saving both time and energy. The effect is also visible in the surge speed and heading of the vessel; yielding smoother behavior across all tests. Figs. 4(b) and 4(d) further highlight the differences, as the vessel failed its docking without bumpless transfer. Table 2 quantifies the improvement in heading angle, which is an important metric in docking situations as there is a large emphasis on precision. Note that these speeds are at the border of what conventional DP systems operate in, and are meant to showcase challenging scenarios where bumpless transfer increases the vessel's robustness and safety. From an operating standpoint however, it is a realistic scenario. Ideally one wants to avoid the vessel excessively slowing down before initiating docking, as one wants to utilize the speed from transit for better energy efficiency. Bumpless transfer facilitates this, docking both faster and more efficiently while keeping a lower surge velocity error, seen in Table 3. Furthermore, it helps ease the strain on the actuators, as bumpless transfer reduces the load significantly.

### 5.3. Dock-to-dock task

Below, the bumpless transfer functionality will be placed in the context of the dock-to-dock method described in Section 3. These tests will feature wind forces, seeing its effect on a vessel transitioning

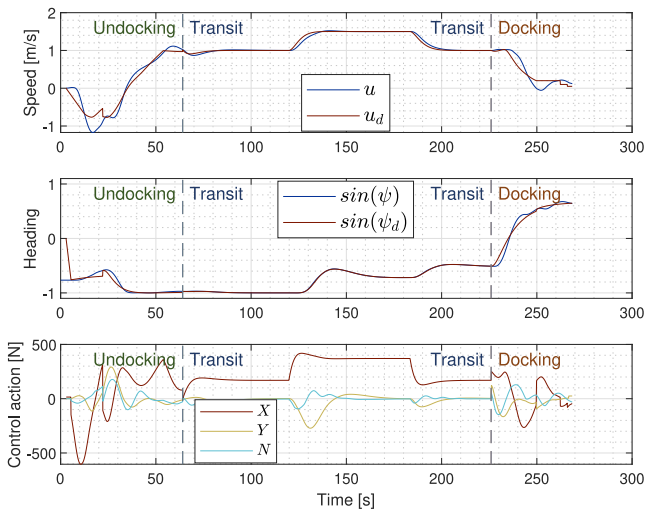


(a) Without bumpless transfer & without wind.

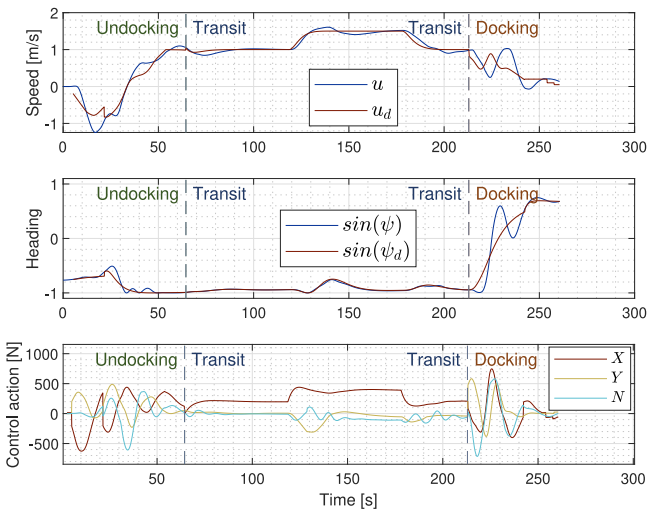


(b) Without bumpless transfer & with wind.

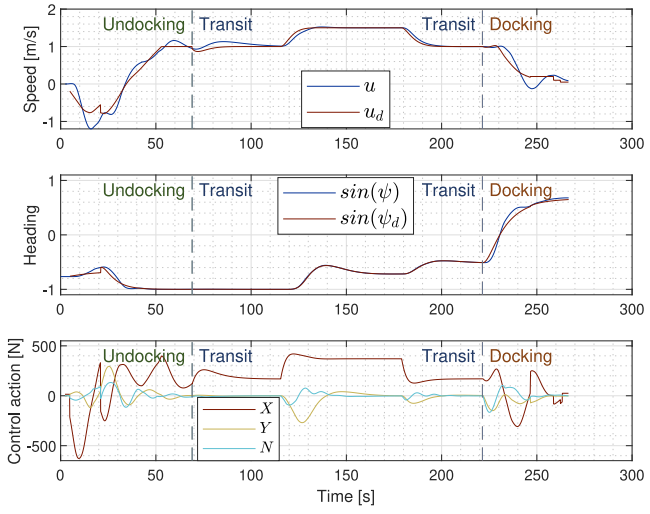


(c) With bumpless transfer & without wind.

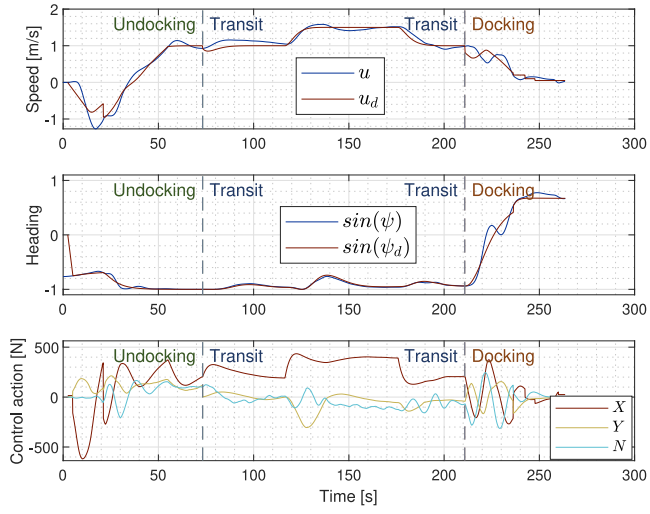


(d) With bumpless transfer & with wind.

**Fig. 6.** Plots of the surge speed, heading, and control action for the different dock-to-dock tests.

abruptly between independent control regimes, and when it transitions with bumpless transfer functionality. The wind is heading south-east at 135° degrees with a speed of 4.0 m/s. This combination was chosen due to this wind angle being one of the more challenging ones, hitting the vessel perpendicular at UNDOCKING and TRANSIT, and diagonally behind during DOCKING. Note that several different wind variations have been tested in simulations, both with changes in the magnitude and direction. The planned route for the dock-to-dock test is depicted in Fig. 5, showing the vessel's position at the waypoints listed in Table 4. The trajectory in Fig. 5 is taken from a bumpless transfer test without any wind.

Without any wind influence, there is not much difference between the cases without- and with bumpless transfer, seen in Figs. 6(a) and 6(c). This is due to the waypoint placements and the transition speed following the proposed method in Section 3; having sufficient waypoint spacing and comfortable transition speeds. This is reflected in Table 5, where there is little to no difference in surge velocity error. Consequently, the main difference is observed in the control action being continuous with bumpless transfer during the transitions. However, once wind forces are present the benefits of bumpless transfer become apparent. This is most notable in the TRANSIT to DOCKING transition, where the oscillations in speed and heading in Fig. 6(b) are heavily reduced with bumpless transfer enabled, seen in Fig. 6(d). The improvements also come in the form of efficiency, as the amplitude of the forces are significantly lowered. In the case of the surge force $X$, it is halved,

**Table 4**
Table showing the waypoints used for the dock-to-dock simulation depicted in Fig. 5. The initial state is [58, 41, −138°].

| UNDOCKING [North, East , $\psi$] | TRANSIT [North, East , $U$] | DOCKING [North, East , $\psi$] |
|---|---|---|
| [63.5, 55.3, −138] | [72.3, −28.5, 1.0] | [−45.5, −119.5, 138] |
| [71.5, 8.7, −90] | [9.3, −92.4, 1.5] | [−47, −118, 138] |
| | [−30.6, −116.6, 1.0] | |

**Table 5**
Table showing the minimum- and maximum values, as well as the RMSE of the surge velocity error from the different dock-to-dock tests. All values are given in m/s.

| | Min value | Max value | RMSE |
|---|---|---|---|
| **Without bumpless** | | | |
| Without wind | −0.41 | 0.34 | 0.11 |
| With wind | −0.63 | 0.55 | 0.17 |
| **With bumpless** | | | |
| Without wind | −0.43 | 0.33 | 0.12 |
| With wind | −0.52 | 0.36 | 0.14 |

**Table 6**
Table showing the minimum- and maximum values, as well as the RMSE of the heading error from the different dock-to-dock tests. All values are given in degrees.

| | Min value | Max value | RMSE |
|---|---|---|---|
| **Without bumpless** | | | |
| Without wind | −9.12 | 9.27 | 2.96 |
| With wind | −35.0 | 38.26 | 9.43 |
| **With bumpless** | | | |
| Without wind | −7.81 | 9.12 | 2.81 |
| With wind | −17.60 | 12.87 | 4.24 |

going from ∼ 700 N to ∼ 350 N with bumpless transfer. Its effect on the heading angle is especially prominent, reducing the RMSE from 9.43° to 4.24° (see Table 6).

## 6. Conclusion

Transitioning between independent controllers in a multi-controller system introduces numerous challenges. These challenges come from discontinuous jumps in the control action, misaligned references from the different guidance laws, and external forces affecting the vessel during transitions. Bumpless transfer is a general method for ensuring continuity or smoothness during these transitions. The solution proposed in this paper uses the integral action of the receiving controller to avoid jumps in control action. This is done enforcing the control action of the two controllers to be equal at the time of transition and solving for the integrator state value. This bumpless transfer solution was tested in the context of an autonomous passenger ferry using the milliAmpere simulator as a test platform. A dock-to-dock method using a state machine approach was implemented, taking the vessel through the three stages of ferry operations, UNDOCKING, TRANSIT, and DOCKING using different control regimes for the various phases. Previous work has validated both the transit and docking controllers in field experiments, demonstrating similar behavior to the simulator. As the proposed method operates as a state machine, these controllers can be independently replaced or altered. Simulation results demonstrate that the proposed implementation successfully combines independent control regimes, taking the vessel from one dock to another. Testing highlighted the importance of bumpless transfer functionality, especially when transitioning from higher to lower speeds. Bumpless transfer also provides increased robustness to environmental forces, reducing their impact when transitioning between the control regimes.

However, as bumpless transfer uses the integrator to compensate for jumps in control action, it may lead to a wind-down period that can affect the vessel's performance. A possible solution is to have an intermediate reference speed equal to the vessel's speed after transitioning, avoiding reference changes while the integrator unwinds. The dock-to-dock method also relies on knowledge of the local conditions the vessel will operate in. These local conditions are usually known for passenger ferries, however, different weather conditions can affect the waypoint placements.

## CRediT authorship contribution statement

**Jens Emil Walmsness:** Methodology, Experiment planning and design, Dataset processing and analysis, Software, Validation, Writing – original draft. **Håkon Hagen Helgesen:** Methodology, Writing – original draft, Conceptualization, Planning, Supervision. **Stefan Larsen:** Software, Formal analysis. **Giorgio Kwame Minde Kufoalor:** Writing – original draft, Conceptualization, Supervision. **Tor Arne Johansen:** Writing – original draft, Conceptualization, Supervision.

## Declaration of competing interest

The authors declare that they have no known competing financial interests or personal relationships that could have appeared to influence the work reported in this paper.

## Data availability

Data will be made available on request.

## Acknowledgment & Funding

This work was supported by the Research Council of Norway with project number 296630. It was also in part supported by the Research Council of Norway through the Centres of Excellence funding scheme, project number 223254. The authors are grateful for the cooperation with Maritime Robotics. The authors would also like to thank Simen Krantz Knudsen for significant contributions in the software development.

## References

Antão, P., Soares, C.G., 2019. Analysis of the influence of human errors on the occurrence of coastal ship accidents in different wave conditions using Bayesian Belief Networks. Accid. Anal. Prev. 133, 105262. http://dx.doi.org/10.1016/j.aap.2019.105262.

Aström, K.J., Hägglund, T., 1995. PID Controllers, second ed. The Instrumentation, Systems, and Automation Society, ISA.

Bitar, G., Eriksen, B.-O.H., Lekkas, A.M., Breivik, M., 2021. Three-phase automatic crossing for a passenger ferry with field trials. In: 2021 European Control Conference. ECC, IEEE, pp. 2271–2277.

Bitar, G., Martinsen, A.B., Lekkas, A.M., Breivik, M., 2020. Two-stage optimized trajectory planning for ASVs under polygonal obstacle constraints: Theory and experiments. IEEE Access 8, 199953–199969.

Blendermann, W., 1994. Parameter identification of wind loads on ships. J. Wind Eng. Ind. Aerodyn. 51 (3), 339–351.

Chen, C., Delefortrie, G., Lataire, E., 2021. Effects of water depth and speed on ship motion control from medium deep to very shallow water. Ocean Eng. 231, 109102. http://dx.doi.org/10.1016/j.oceaneng.2021.109102, URL: https://www.sciencedirect.com/science/article/pii/S0029801821005370.

Fossen, T., 2021. Handbook of Marine Craft Hydrodynamics and Motion Control, second ed. John Wiley & Sons.

Fossen, T.I., Breivik, M., Skjetne, R., 2003. Line-of-sight path following of underactuated marine craft. IFAC Proc. Vol. 36 (21), 211–216.

Helgesen, H.H., Kristiansen, K.S., Vik, B., Johansen, T.A., 2022. Quay contact detection for ships using motion sensors and machine learning. IFAC-PapersOnLine IFAC Conference on Control Applications in Marine Systems, Robotics, and Vehicles (CAMS).

Hu, B., Liu, X., Jing, Q., Lyu, H., Yin, Y., 2022. Estimation of berthing state of maritime autonomous surface ships based on 3D LiDAR. Ocean Eng. 251, 111131. http://dx.doi.org/10.1016/j.oceaneng.2022.111131, URL: https://www.sciencedirect.com/science/article/pii/S002980182200542X.

Kinnaert, M., Delwiche, T., Yamé, J., 2009. State resetting for bumpless switching in supervisory control. In: 2009 European Control Conference. ECC, IEEE, pp. 2097–2102.

Knudsen, S., 2021. Model Validation and Berthing of an Autonomous Ferry (Master Thesis). NTNU.

Larsen, S., 2022. Automatic Docking Algorithm for Passenger Ferries (Master Thesis). NTNU.

Lekkas, A.M., Fossen, T.I., 2012. A time-varying lookahead distance guidance law for path following. IFAC Proc. Vol. 45 (27), 398–403.

Lourenco, J., Lemos, J., 2006. Learning in multiple model adaptive control switch. IEEE Instrum. Measur. Mag. 9 (3), 24–29.

Martinsen, A.B., Bitar, G., Lekkas, A.M., Gros, S., 2020. Optimization-based automatic docking and berthing of ASVs using exteroceptive sensors: Theory and experiments. IEEE Access 8, 204974–204986.

Nguyen, T.D., Sørensen, A.J., Quek, S.T., 2008. Multi-operational controller structure for station keeping and transit operations of marine vessels. IEEE Trans. Control Syst. Technol. 16 (3), 491–498.

Nomoto, K., Taguchi, K., Honda, K., Hirano, S., 1956. On the steering qualities of ships. J. Zosen Kiokai 1956 (99), 75–82.

Öztürk, Ü., Akdağ, M., Ayabakan, T., 2022. A review of path planning algorithms in maritime autonomous surface ships: Navigation safety perspective. Ocean Eng. 251, 111010. http://dx.doi.org/10.1016/j.oceaneng.2022.111010, URL: https://www.sciencedirect.com/science/article/pii/S0029801822004334.

Pasamontes, M., Álvarez, J.D., Guzmán, J.L., Berenguel, M., 2010. Bumpless switching in control-A comparative study. In: 2010 IEEE 15th Conference on Emerging Technologies & Factory Automation. ETFA 2010, IEEE, pp. 1–8.

Pasamontes, M., Álvarez, J., Guzmán, J., Lemos, J., Berenguel, M., 2011. A switching control strategy applied to a solar collector field. Control Eng. Pract. 19 (2), 135–145.

Pedersen, A.A., 2019. Optimization Based System Identification for the Milliampere Ferry (Master Thesis). NTNU.

Saelid, S., Jenssen, N.A., Balchen, J.G., 1983. Design and analysis of a dynamic positioning system based on Kalman filtering and optimal control. IEEE Trans. Autom. Control 28 (3), 331–339.

Tanko, M., Burke, M., 2017. Transport innovations and their effect on cities: The emergence of urban linear ferries worldwide. Transp. Res. Procedia 25, 3957–3970. http://dx.doi.org/10.1016/j.trpro.2017.05.483, World Conference on Transport Research.

Teel, A.R., Kapoor, N., 1997. The $\mathcal{L}_2$ anti-windup problem: Its definition and solution. In: 1997 European Control Conference. ECC, IEEE, pp. 1897–1902.

Wang, L., Li, S., Liu, J., Wu, Q., Negenborn, R.R., 2022. Ship docking and undocking control with adaptive-mutation beetle swarm prediction algorithm. Ocean Eng. 251, 111021. http://dx.doi.org/10.1016/j.oceaneng.2022.111021.

Zaccarian, L., Teel, A.R., 2002. A common framework for anti-windup, bumpless transfer and reliable designs. Automatica 38 (10), 1735–1744.